Journal of Hydrology: Regional Studies 37 (2021) 100920

Contents lists available at ScienceDirect

Journal of Hydrology: Regional Studies

journal homepage: www.elsevier.com/locate/ejrh

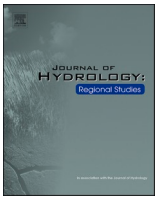

Does non-stationarity of extreme precipitation exist in the Poyang Lake Basin of China?

Xiangyong Lei [a,b], Lu Gao [a,b,c,d,*], Miaomiao Ma [e], Jianhui Wei [f], Ligang Xu [g], Lan Wang [h], Hui Lin [h]

[a] *Institute of Geography, Fujian Normal University, Fuzhou, 350007, China*
[b] *College of Geographical Science, Fujian Normal University, Fuzhou, 350007, China*
[c] *Fujian Provincial Engineering Research Center for Monitoring and Accessing Terrestrial Disasters, Fujian Normal University, Fuzhou, 350007, China*
[d] *State Key Laboratory for Subtropical Mountain Ecology of the Ministry of Science and Technology and Fujian Province, Fujian Normal University, Fuzhou, 350007, China*
[e] *China Institute of Water Resources and Hydropower Research, Beijing, 100038, China*
[f] *Institute of Meteorology and Climate Research, Karlsruhe Institute of Technology, Garmisch-Partenkirchen, 82439, Germany*
[g] *Key Laboratory of Watershed Geographic Science, Nanjing Institute of Geography and Limnology, Chinese Academy of Sciences, Nanjing, 210008, China*
[h] *Fujian Key Laboratory of Severe Weather, Fuzhou, 350001, China*

ARTICLE INFO

Keywords:
Non-stationary
Spatio-temporal variation
Extreme precipitation
Poyang Lake Basin
GAMLSS

ABSTRACT

Study region: Poyang Lake Basin, China.
Study focus: This study aimed to investigate whether there are non-stationary characteristics of extreme precipitation in the Poyang Lake Basin (PLB) of China, and the trends of non-stationary characteristics from 1959 to 2019. The spatio-temporal variations of extreme precipitation were analysed from three fundamental aspects: duration, frequency, and intensity, based on the pre-whitening Mann-Kendall (PWMK) test. Non-stationary variations and the risk of extreme precipitation were investigated based on the generalized additive models for location, scale, and shape (GAMLSS).
New hydrological insights for the region: (1) the intensity and frequency of extreme precipitation increased significantly, whereas there was a significant decrease in extreme precipitation duration in the PLB. (2) The duration of extreme precipitation showed significant non-stationary characteristics in the western PLB. At the Nanchang site, 83.3 % of the extreme precipitation intensity indices showed non-stationary characteristics. The RX1day (maximum 1-day precipitation amount) and RX5day (maximum 5-day precipitation amount) increased significantly for different return periods under non-stationary conditions in the northwestern PLB. (3) The risk of extreme precipitation can be captured using the GAMLSS. The stationary method underestimated the extreme precipitation intensity (e.g., RX1day) compared to the GAMLSS for longer return periods in the PLB. More attention should be paid to the increase and fluctuation of the return period of extreme precipitation caused by the mean non-stationarity and variance non-stationarity.

* Corresponding author at: Institute of Geography, Fujian Normal University, Fuzhou, 350007, China.
E-mail address: l.gao@foxmail.com (L. Gao).

https://doi.org/10.1016/j.ejrh.2021.100920
Received 10 May 2021; Received in revised form 15 August 2021; Accepted 9 September 2021
Available online 15 September 2021

1. Introduction

Climate change (particularly extreme weather events) has attracted considerable attention in recent decades (Gudmundsson et al., 2021; Zou et al., 2021). The Fifth Intergovernmental Panel on Climate Change (IPCC) report provided clear evidence of global warming. From 1880 to 2012, the average global surface temperature increased by approximately 0.85 °C (IPCC, 2014). Compared with the average climate, extreme climatic events are more sensitive to climate change (Gao et al., 2017) and the trend of change is stronger (Khan et al., 2020). Therefore, in the context of global warming, the intensity and frequency of extreme events have changed significantly (Ali et al., 2018; Gao et al., 2020; Kundzewicz et al., 2020). In recent years, there has been an increase in the frequency of extreme high temperature and extreme precipitation events (Alexander, 2016) and extreme precipitation events are positively correlated with temperature increases (Ali et al., 2018; Gao et al., 2020). The global increase in the frequency and intensity of extreme precipitation events not only leads to serious natural hazards such as floods (Tang et al., 2021) and landslides and debris flows (Ingram, 2016), but also causes substantial human and economic losses (Lu et al., 2021).

Global extreme weather event variability and trends have shown significant changes, and many previous studies have shown that China experiences frequent extreme precipitation events (Li and Chen, 2021; Lu et al., 2020; Zhou et al., 2021). As the largest freshwater lake in China, Poyang Lake has strategic importance in sustaining the surrounding ecological environment. Several studies have found that climate change and human activity have caused more extreme precipitation events and floods in the Poyang Lake Basin (PLB) in the recent decades (Li et al., 2021; Ma et al., 2021; Zhu et al., 2020), which has severely affected the stability of the surrounding environment (Zhan et al., 2019). The effects of human activities on climate change mainly correspond to the frequent use of fossil fuels, massive greenhouse gas emissions, land use and land cover change, and construction of reservoirs (Xin et al., 2019). In addition, previous studies have shown that the East Asian Summer Monsoon (EASM) (Zou and Ren, 2015), El Niño/Southern Oscillation (ENSO), North Atlantic Oscillation (NAO), Indian Ocean Dipole (IOD), and Pacific Decadal Oscillation (PDO) are significantly associated with extreme precipitation events in the PLB, particularly ENSO (Xiao et al., 2015).

Li and Hu (2019) used a group of extreme precipitation-related indices based on the Mann–Kendall (MK) trend test (Kendall, 1975; Mann, 1945) and found an intensified trend of extreme precipitation events in the PLB during 1960–2012. Zhang et al. (2015) used 15 rain gauges and the MK trend test and found that precipitation changes intensified, as reflected by increased precipitation extremes. Most existing studies are based on the MK trend test to identify whether significant trends exist in hydro-meteorological time series. However, there are autocorrelation effects in the hydrometeorological time series, which can lead to errors in the trends (Das and Scaringi, 2021; O'Brien et al., 2021).

Moreover, the stationary and non-stationary characteristics of extreme precipitation events have become a hot issue in climate change research (Sun et al., 2018). Studies based on the stationarity assumption indicated that sample series obeyed the same distribution in the past, present, and future. However, in a changing environment, climate change and human activities significantly influence the intensity, frequency, and duration of extreme precipitation events (Gao et al., 2018) so the conventional stationarity hypothesis is no longer suitable for flood risk assessment and hydrological project design (Gao et al., 2017, 2018). However, most existing flood protection design standards are based on assumptions of stationarity when calculating storm return periods, which can lead to distortion of the standards (Lu et al., 2020; Mirdashtvan and Mohseni Saravi, 2020). Therefore, when studying extreme precipitation, non-stationary characteristics need to be tested to ensure the accuracy of the results (Sun et al., 2018). Rigby and Stasinopoulos (2005) proposed a non-stationary analysis model called generalized additive models for location, scale, and shape (GAMLSS), which has been widely used for the simulation and attribution analysis of runoff changes by constructing linear, nonlinear, parametric, and non-parametric relationships between distribution function parameters and multiple explanatory variables. Chen et al. (2021) used the peak flow series from 158 gauges in the UK based on GAMLSS. Moreover, previous studies have shown that GAMLSS has good applicability in investigating the non-stationary characteristics of extreme precipitation in the southeast coastal region of China (Gao et al., 2017).

It is important to assess the trend of extreme precipitation events and analyze the stationary and non-stationary characteristics of PLB to reduce the effects of natural disaster reduction and management of water resources. To achieve this, the prewhitening MK (PWMK) test (Yue and Wang, 2002), which eliminates autocorrelation in meteorological and hydrological series, was selected for trend testing. The GAMLSS, which is based on the location, scale, and shape parameters, was selected for non-stationary analysis. The objectives were to: 1) analyze the spatio-temporal variation in extreme precipitation, 2) detect the non-stationary characteristics of extreme precipitation, and 3) investigate the recurrence risk of extreme precipitation events. The outcome of this study can provide effective scientific support for reducing the effects of extreme precipitation events in the PLB. The remainder of this paper is organized as follows: Section 2 describes the data and methods used in this study, Section 3 elaborates the results analysis, and the discussion and conclusions are presented in Sections 4 and 5, respectively.

2. Data and methods

2.1. Meteorological observations

As an important storage lake in the Yangtze River Basin, Poyang Lake plays an important supplementary role in maintaining water sources and protecting ecological diversity (Lei et al., 2021). The PLB extends between 113.74–118.47 ° E and 24.57–30.01 ° N, with a drainage basin area of 16.22×10^4 km^2. The PLB has a subtropical monsoon climate with an average annual precipitation of 1664 mm. The PLB has low elevation in the middle and high elevations, including high mountains, hills, and plains. The lake receives water flows mainly from five rivers: Ganjiang, Fuhe, Xinjiang, Raohe, and Xiushui.

There are 16 meteorological stations conducting long-term consecutive measurements in the PLB (Fig. 1). The measurements were obtained from the China Meteorological Data Sharing Service System of the National Meteorological Information Center (http://data.cma.cn/) for 1959–2019. All the selected stations can reflect the rainfall trend, with no gaps exceeding two consecutive weeks. The quality of the observations was rigorously tested by the provider, and we performed quality control and error analysis on all data before conducting the analysis to ensure the authenticity and accuracy of the data.

2.2. Methods

2.2.1. Extreme precipitation indices

The extreme climate indices are a series of climate indices provided by the Expert Team on Climate Change Detection Monitoring and Indices (ETCCDMI), based on daily temperature and precipitation data. Extreme precipitation indices were calculated to detect the non-stationary characteristics of extreme precipitation events (Table 1). These indices were computed using the RClimDex software (Zhang and Yang, 2004). The calculation process of RClimDex includes data quality control, homogenization tests, and index calculations. There are 11 extreme precipitation indices recommended by ETCCDMI, and Rnn was modified to R1mm and R50 mm in this study.

Based on different classification criteria, the extreme precipitation indices can be divided into different categories, which can be classified into monthly extreme precipitation indices and annual extreme precipitation indices based on different time scales, and into absolute threshold indices and relative threshold indices based on different threshold classification methods (Alexander et al., 2019). For example, Croitoru et al. (2013) classified extreme precipitation indices into two categories based on frequency and intensity. Yao et al. (2020) classified extreme precipitation indices into four categories based on intensity, percentile threshold, frequency, and duration. Based on the rainfall characteristics of the study area, we classified these 12 extreme precipitation indices into the following three categories: 1) duration indices, including CDD and CWD; 2) frequency indices, including R1mm, R10 mm, R20 mm, and R50 mm; and 3) intensity indices, including RX1day, RX5day, SDII, R95p, R99p, and PRCPTOT.

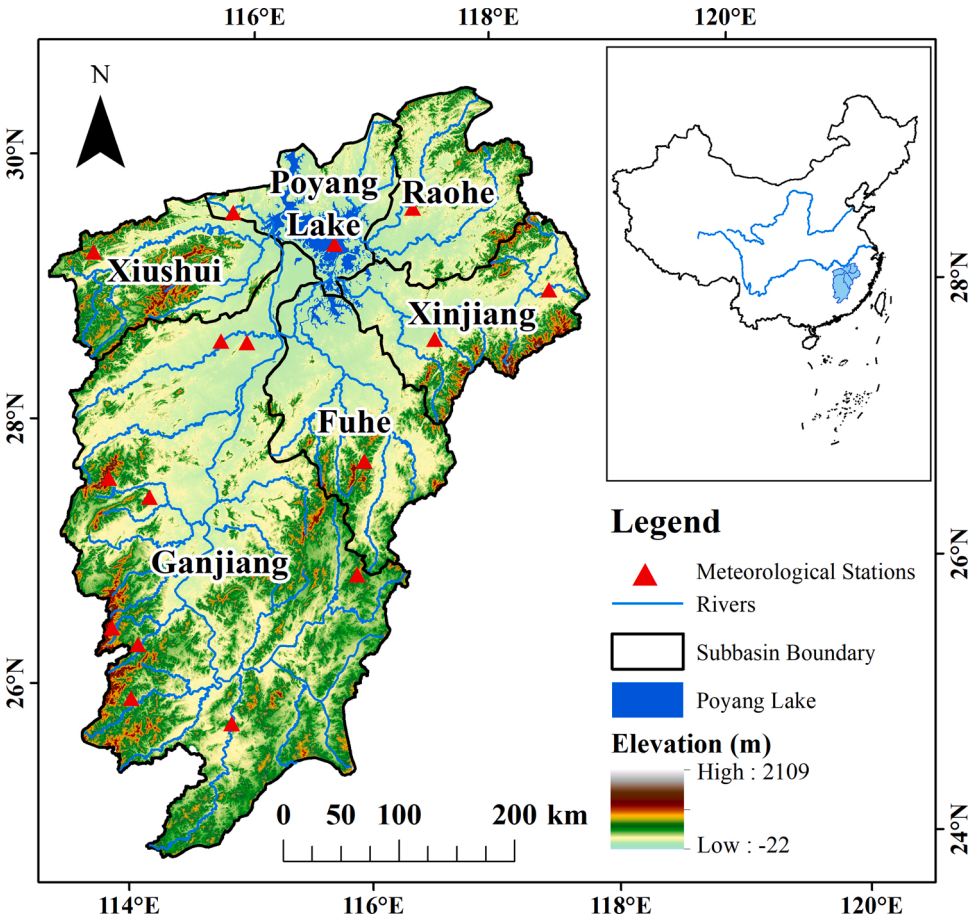

Fig. 1. Location of the study area and meteorological stations.

Table 1
Extreme precipitation indices considered in this study.

Index	Indicator name	Description	Units
RX1day	Max 1-day precipitation amount	Monthly maximum 1-day precipitation	mm
RX5day	Max 5-day precipitation amount	Monthly maximum consecutive 5-day precipitation	mm
SDII	Simple daily intensity index	Annual total precipitation divided by the number of wet days (defined as precipitation $>=1.0$ mm) in the year	mm/day
R1mm	Number of wet days	Annual count of days when precipitation $>=1$ mm	Days
R10mm	Number of heavy precipitation days	Annual count of days when precipitation $>=10$ mm	Days
R20mm	Number of very heavy precipitation days	Annual count of days when precipitation $>=20$ mm	Days
R50mm	Number of extreme heavy precipitation days	Annual count of days when precipitation $>=50$ mm	Days
CDD	Consecutive dry days	Maximum number of consecutive days with daily precipitation <1mm	Days
CWD	Consecutive wet days	Maximum number of consecutive days with daily precipitation $>=1$ mm	Days
R95p	Very wet days	Annual total precipitation when daily precipitation >95th percentile	mm
R99p	Extremely wet days	Annual total precipitation when daily precipitation >99th percentile	mm
PRCPTOT	Annual total wet days precipitation	Annual total daily precipitation in wet days	mm

2.2.2. Trend analysis

The MK test is a non-parametric test recommended by the World Meteorological Organization (WMO) for time-series analysis and is widely used for trend testing of hydrological and meteorological elements. However, in the application process, the autocorrelation of hydrological and meteorological elements often causes the elements with insignificant trends to become significant. Thus, it should be noted that the results of the MK test were affected by autocorrelation of the time series. It is essential to keep the time series serially independent before performing the trend test. The PWMK test (Yue and Wang, 2002), which can eliminate autocorrelation in the series and maintain consistency with the overall trend of the MK test results, was considered for trend testing in this study. Previous studies have used the prewhitening procedure before trend detection (O'Brien et al., 2021; Wu et al., 2021; Xu and Tang, 2021). The results showed that this method is more reasonable than the MK test and improves the accuracy of the trend test. In this study, the pre-whitening procedure was applied by the following steps:

First, eliminating the linear trend of raw series.

$$Y_t = X_t - \beta_t \tag{1}$$

where Y_t, X_t and β_t are the de-trended series, raw series value, and linear regression slope of the trend in the raw series at time t, respectively.

Second, removing the autocorrelation term from the de-trended series.

$$Y_t^{'} = Y_t - r_1 Y_{t-1} \tag{2}$$

where r_1 is the lag-1 serial correlation coefficient of the de-trended series and $Y_t^{'}$ is the de-trended and pre-whitened series, called the residual series.

Finally, we added the linear trend that was eliminated in the first step back to the de-trended or residual series.

$$Y^{''}{}_t = Y_t^{'} + \beta_t \tag{3}$$

where $Y^{''}{}_t$ is the pre-whitened series.

2.2.3. GAMLSS model

The GAMLSS model can establish the relationship between the statistical parameters of the response variables (location, scale, shape, etc.) and explanatory variables based on fitting the location, scale, and shape parameters with an addable semi-parametric or non-parametric term, or a random-effects term (Rigby and Stasinopoulos, 2005). The ability to introduce multiple explanatory variables is a remarkable advantage of the GAMLSS.

In this study, we used a semi-parametric GAMLSS model. Suppose there are n independent observations, y_i ($i = 1, \cdots, n$), which follow a distribution of $F_y(y_i\theta_i)$. In this case, θ_i corresponds to the location parameter (mean (Mn), median, etc.), the scale parameter (variance (Var), mean square, etc.), and the shape parameter (skewness coefficient, kurtosis coefficient), where $\theta_{iT} = (\theta_{i1}, \theta_{i2}, \cdots, \theta_{ik})$ represents the k parameters (position, scale, and shape) vector, and k is usually less than 4. The formula is as follows:

$$g_k(\theta_k) = X_k\beta_k + \sum_{j=1}^{m} h_{jk}(x_{jk}) \tag{4}$$

where θ_k is a vector of length n, X_k is an $n \times m$ matrix of explanatory variables, and β_k is a vector of parameters of length m. $h_{jk}(.)$ represents the functional relationship between the distribution parameters and the explanatory variables x_{jk}. This model is widely used for risk assessment of extreme precipitation events and has been shown to outperform traditional distribution models (Chen et al., 2021; Gao et al., 2018). Here, we briefly describe the application of the GAMLSS model in this study. The changes in Mn and Var of the

extreme precipitation series indicate that they exhibit non-stationary characteristics (Gao et al., 2018). Therefore, the Mn and Var of the extreme precipitation series were used to characterize the location and scale parameters in the GAMLSS model, respectively. Moreover, the effect of the random term on the model was not considered in this study. The functional relationship between the statistical parameters mean θ_1 and variance θ_2 and the unique explanatory variable time t is as follows:

$$g_1(\theta_1) = t\beta_1 \tag{5}$$

$$g_2(\theta_2) = t\beta_2 \tag{6}$$

The common types of distribution functions are listed in Table 2. The parameters of the distribution functions are Mn and Var of the extreme precipitation series.

Common trend line-type expressions are summarized in Table 3. In this study, we considered a series in which Mn and Var exhibit a non-linear trend with non-stationarity.

3. Results

3.1. Spatio-temporal variation in extreme precipitation

3.1.1. Temporal variation of extreme precipitation indices

Fig. 2 illustrates the temporal variation of extreme precipitation indices from 1959 to 2019 in the PLB. In general, all indices except CDD, CWD, and R1mm showed a linearly increasing trend. The duration indices decreased and the intensive and frequent indices increased.

For the duration indices, CDD showed a significant downward trend between 1960 and 1973, with a sudden increase to a peak of 43 days in 1974, and showed a slow downward trend thereafter. Similar to CDD, CWD showed a decreasing trend until 1975, with a peak of 24 days in 1999 and a minimum of 9 days in 1989, 1991, and 2006.

For the frequency indices, the decreasing trend of R1mm was not significant, reaching a minimum value of 148 days in 2003 and gradually increasing thereafter. R10 mm, R20 mm and R50 mm all showed an upward trend, with R20 mm showing largest upward trend. Note that some years have zero values of R50 mm during the time series, which was due to the limitations of the Thiessen polygon interpolation.

For the intensity indices, both R95p and R99p showed a long-term increasing trend in the time series. R95p showed a clear upward trend after 1978, but showed decreasing trend during 2000–2009 and showed an upward trend thereafter. In contrast, the fluctuating trend of R99p was highly variable, with a total of 16 years with zero values, but with extreme values of 300 mm in both 1994 and 1998, and a continuous increasing trend after 2017. We also found that the trends of RX1day and RX5day were similar, but that of RX5day was more volatile. RX1day reached a maximum of 101 mm in 2001. RX5day showed a decreasing trend from 1967 to 1979 and increased thereafter. SDII varied between 6.8 mm/day in 1963 and 11.7 mm/day in 1998, with a significant increase over the entire study period. There was a visible upward trend in PRCPTOT, but a low-value range was observed between 2000 and 2009.

Table 4 illustrates that, except for CDD and CWD, the other extreme precipitation indices showed an increasing trend at different confidence levels from 1959 to 2019. For R20 mm, R95p, and SDII, these indices showed a significant increasing trend at the 0.1 significance level.

3.1.2. Spatial variation of extreme precipitation indices

The intensity and frequency of extreme precipitation indices in the PLB showed an increasing trend during the past 61 years, while the duration showed a decreasing trend (Fig. 3). In terms of the duration of extreme precipitation indices, more stations showed decreased trends in duration indices than those with increasing trends. The frequency indices showed an increasing trend for all stations except Ganzhou and Guangchang. The intensity indices showed an increasing trend at all stations except Boyang, with Yichun and Nancheng reaching a significance level of 0.05. Geographically, these results illustrate that the extreme precipitation intensity and frequency over the central PLB have increased. However, extreme precipitation events in the northwestern and southwestern regions of the basin showed less variability.

Fig. 4 shows the PWMK trend for 12 extreme precipitation indices in PLB at different confidence levels from 1959 to 2019. For the

Table 2
Information on distribution functions.

Distribution function	Abbreviation	Number of parameters
Gamma	GA	2
Gumbel	GU	2
Log-Normal	LOGNO	2
Logistic	LO	2
Normal	NO	2
Inverse Gamma	IGAMMA	2
Inverse Gaussian	IG	2
Reverse Gumbel	RG	2
Weibull	WEI3	2

Table 3
Information on line type expressions.

No.	Trendline type	Expressions	Characteristic
1	m linear trend, σ no trend	$m = m_0 + m_1 t, \sigma = \sigma_0$	stationary
2	m no trend, σ linear trend	$m = m_0, \sigma = \sigma_0 + \sigma_1 t$	stationary
3	m parabolic trend, σ no trend	$m = m_0 + m_1 t + m_2 t^2, \sigma = \sigma_0$	non-stationary
4	m no trend, σ parabolic trend	$m = m_0, \sigma = \sigma_0 + \sigma_1 t + \sigma_2 t^2$	non-stationary
5	m linear trend, σ linear trend	$m = m_0 + m_1 t, \sigma = \sigma_0 + \sigma_1 t$	stationary
6	m parabolic trend, σ linear trend	$m = m_0 + m_1 t + m_2 t^2,$ $\sigma = \sigma_0 + \sigma_1 t$	non-stationary
7	m linear trend, σ parabolic trend	$m = m_0 + m_1 t,$ $\sigma = \sigma_0 + \sigma_1 t + \sigma_2 t^2$	non-stationary
8	m parabolic trend, σ parabolic trend	$m = m_0 + m_1 t + m_2 t^2,$ $\sigma = \sigma_0 + \sigma_1 t + \sigma_2 t^2$	non-stationary

Note: m and σ are the first- and second-order moments of the probability density function, that is, Mn and Var, respectively.

duration indices, CDD and CWD showed increasing trends in the southern and northern parts of the PLB, respectively. For the frequency indices, R1mm showed a decrease in the southern part of PLB and an increase in the northern part. As the threshold increased, an increasing trend from R10 mm to R50 mm across the entire basin was observed. Zhangshu and Nancheng showed a significant increasing trend of R50 mm at 0.05 significance level. Nanxiong and Guangchang were the exceptions. In terms of intensity indices, R95p showed an increasing trend across the basin, and for seven stations it reached the 0.05 significance level. However, compared to the trends at R95p, Boyang and Jinggangshan exhibited increasing trends at R99p. Additionally, at 13 out of 16 stations, RX1day and RX5day were dominated by a not-significant increasing tendency. We observed an overall increasing tendency of the SDII and six stations at 0.05 significance level. PRCPTOT showed an increasing trend at all stations except for Nanxiong.

Table 5 shows that most stations (93.75 %) in the PLB had increasing trends, with the most significant increasing trend in Zhangshu and Jinggangshan. However, there was a decreasing trend in the extreme precipitation indices of about 30 % or more at stations such as Nanxiong, Boyang, and Ji'an.

Table 6 shows that 75 % of the extreme precipitation indices showed increasing trends at each station, with R20 mm, R50 mm, R95p, RX1day, and SDII showing increasing trends at more than 13 stations. Fewer stations showed no trend, and only CWD, R10 mm, R99p, and PRCPTOT showed no trend at individual stations. In contrast, CDD, CWD, and R1mm showed decreasing trend at more than 50 % of stations, with R1mm decreasing at approximately 60 % of the 16 stations.

3.2. Non-stationary variation of extreme precipitation indices

To assess the degree of goodness-of-fit between the statistical model and fitted data, the minimum Akaike information criterion (AIC) value was selected. The results of the optimal GAMLSS model obtained using the AIC criterion (Tables 7–9) showed that more than half of the extreme precipitation indices at 81.25 % of the stations in the PLB exhibited stationary characteristics, and the optimal distribution type was IGAMMA with a line shape of 1, that is, a linear trend in Mn and no trend in Var.

In general, the extreme precipitation indices at each station were dominated by stationary characteristics (Table 8), with a maximum number distribution of IGAMMA and a maximum number linearity of 1. These results indicate that the stations can be divided into three categories: those with significant stationary characteristics (Xiushui, Yichun, Ganzhou, Nanxiong, Jingdezhen, Guixi, Yushan, Nancheng and Guangchang), those with a balance between stationary and non-stationary characteristics (Ji'an, Jinggangshan, Suichuan, Lushan, Boyang, and Zhangshu), and those with significant non-stationary characteristics (Nanchang).

For the stations with significant stationary characteristics, Yichun, Ganzhou, Nanxiong, Guixi, Yushan, and Guangchang all had 10 or more indices showing stationary characteristics, including the Guixi station, with all extreme precipitation indices showing stationary characteristics. Among the stations with balanced stationary and non-stationary characteristics, stations such as Ji'an and Jinggangshan showed non-stationary characteristics with five or more extreme precipitation indices. Only Nanchang had significant non-stationary characteristics of extreme precipitation indices, with 83.3 % of extreme precipitation intensity indices being non-stationary, the most at any individual station.

Overall, the stations were dominated by stationary characteristics with regard to each extreme precipitation index (Table 9). However, certain stations exhibited non-stationary characteristics with regard to each index. In terms of the duration indices, the number of sites with stationary and non-stationary characteristics was similar for CDD and CWD, with both having nine stations exhibiting stationary characteristics. For the frequency indices, R10 mm, R20 mm, and R50 mm, all showed stationary characteristics. The number of stations with non-stationary characteristics in R1mm was 43.75 %. With the exception of RX5day, the intensity indices were classified as having significant stationary characteristics, with each index exhibiting stationary characteristics at more than 10 stations.

With the exception of three indices, R1mm, R10 mm and RX5day, the remaining indices were mostly stationary in the northern part of the basin (Fig. 5). In contrast, the R10 mm, R20 mm, R50 mm, R95p, R99p, SDII, and PRCPTOT indices showed stationary characteristics in the southern part of the PLB.

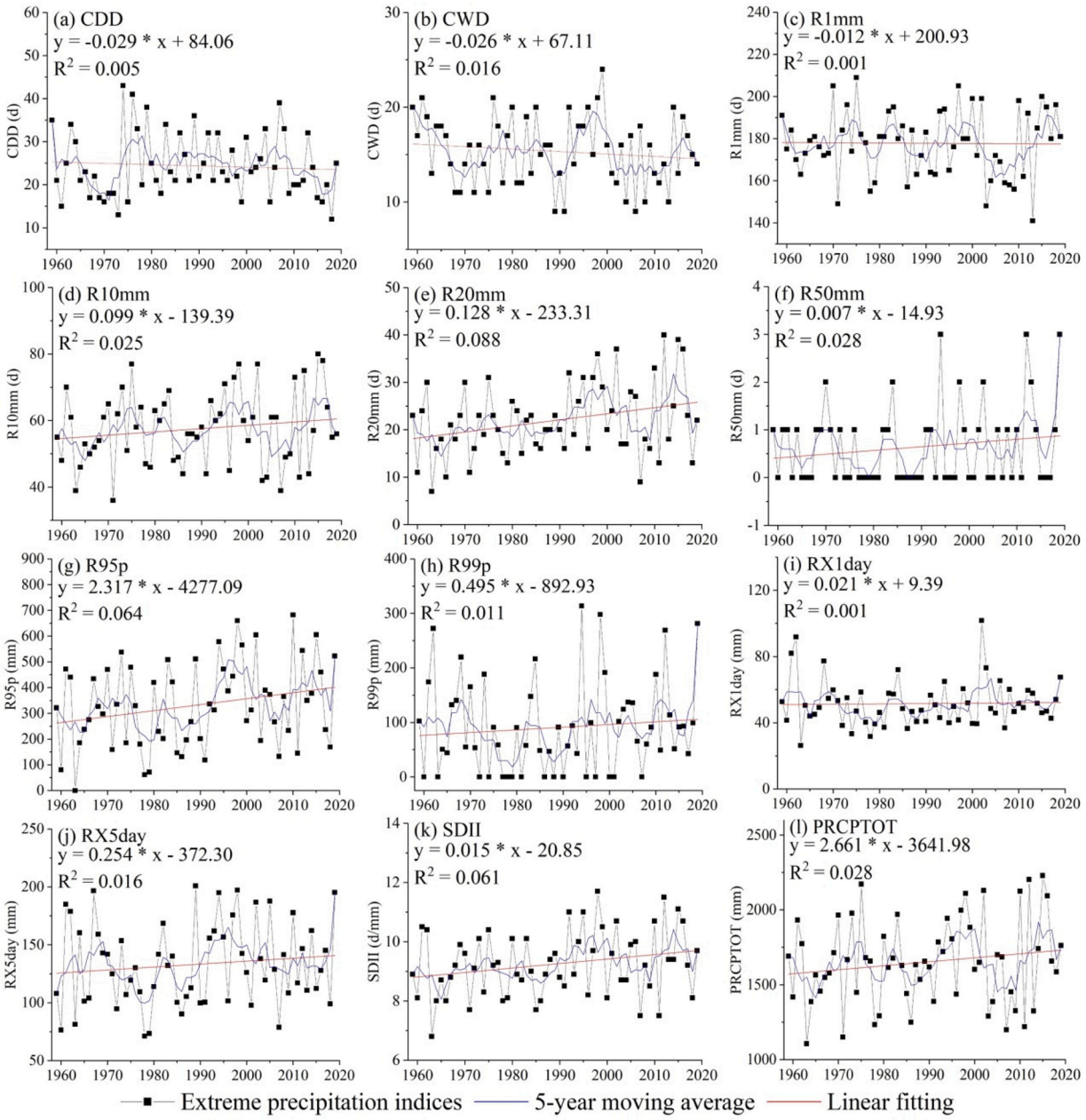

Fig. 2. Variation of extreme precipitation indices in PLB during 1959–2019.

Table 4
PWMK test for extreme precipitation indices.

Index	CDD	CWD	R1mm	R10mm	R20mm	R50mm	R95p	R99p	RX1day	RX5day	SDII	PRCPTOT
PWMK statistic	−0.37	−1.05	0.22	1.16	1.93*	0.57	1.75*	0.82	0.69	0.90	1.76*	1.41

Note : * delineates significance at 0.1 significance level.

Fig. 6 illustrates the PWMK trends for Mn at different confidence levels from 1959 to 2019. The results for Mn were generally consistent with the linear trend (Fig. 2). CDD, CWD, and R1mm showed decreasing trends in the study area. Most of the other indices showed an increasing trend and reached the 0.05 significance level. However, R99p and RX5day showed a decreasing trend and no trend in the northeastern and northwestern areas of the PLB, respectively.

The results of the PWMK trend test for Var at each station (Fig. 7) showed a multivariate trend compared to that of Mn. For the

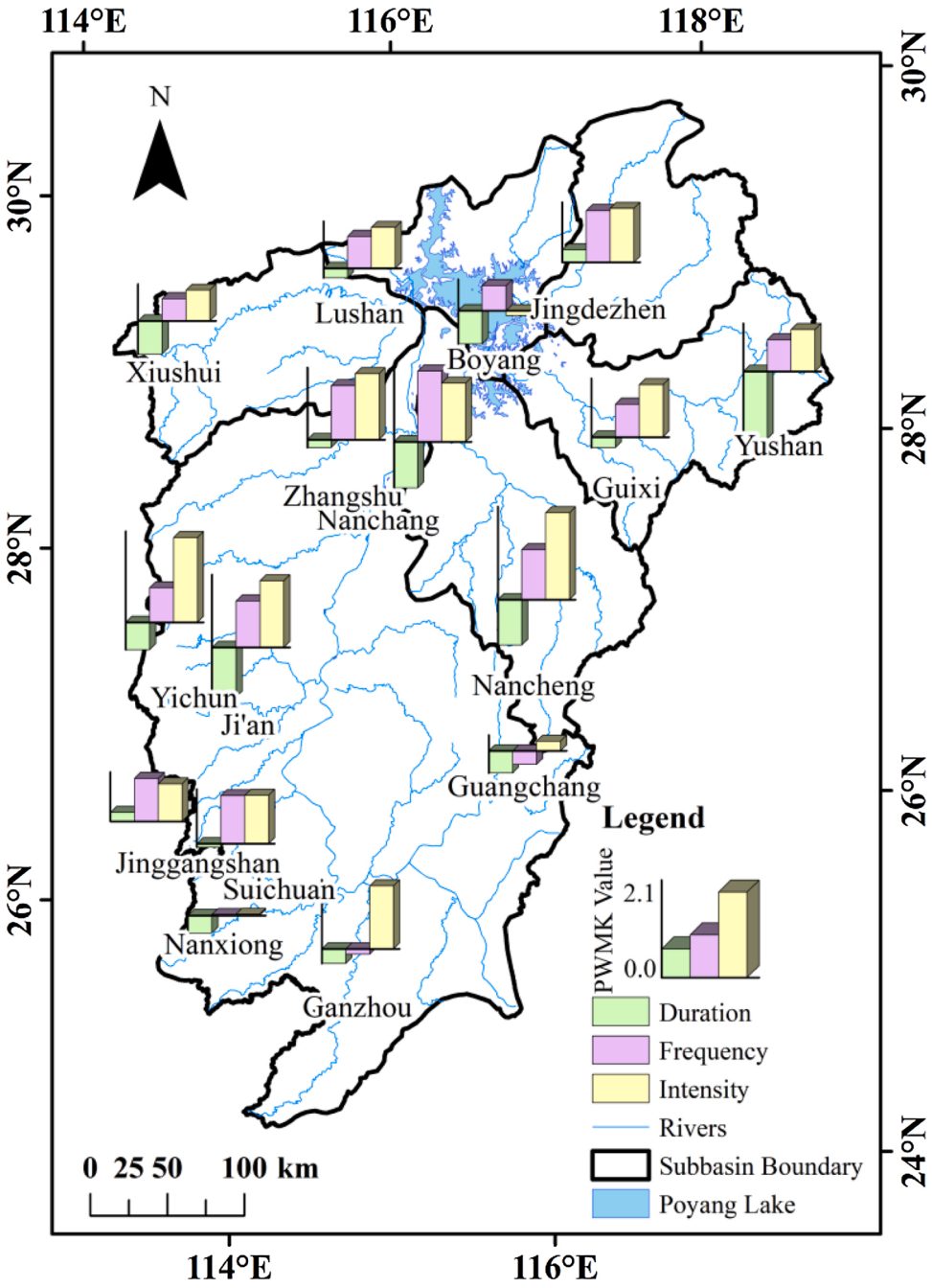

Fig. 3. Spatial distribution of the PWMK test for the duration, frequency, and intensity of extreme precipitation indices in PLB during 1959–2019.

duration indices, CDD and CWD showed decreasing and increasing trends in the western part of the PLB, respectively. The frequency indices primarily showed a decreasing trend, with no more than four stations showing an increasing trend. Among the intensity indices, R95p and R99p showed opposite trends, with the former showing a decreasing trend in the southwestern and northeastern parts of the basin, whereas the latter showed increasing trends at most stations in the basin. The trends for RX1day and RX5day were similar, both showing decreasing trends in the northeastern area of the basin and increasing trends in the southeastern area of the basin. The majority of stations showed a decreasing trend with respect to SDII. PRCPTOT showed a decreasing trend in the northeastern and southwestern parts of the basin and an increasing trend in the southeastern part of the basin.

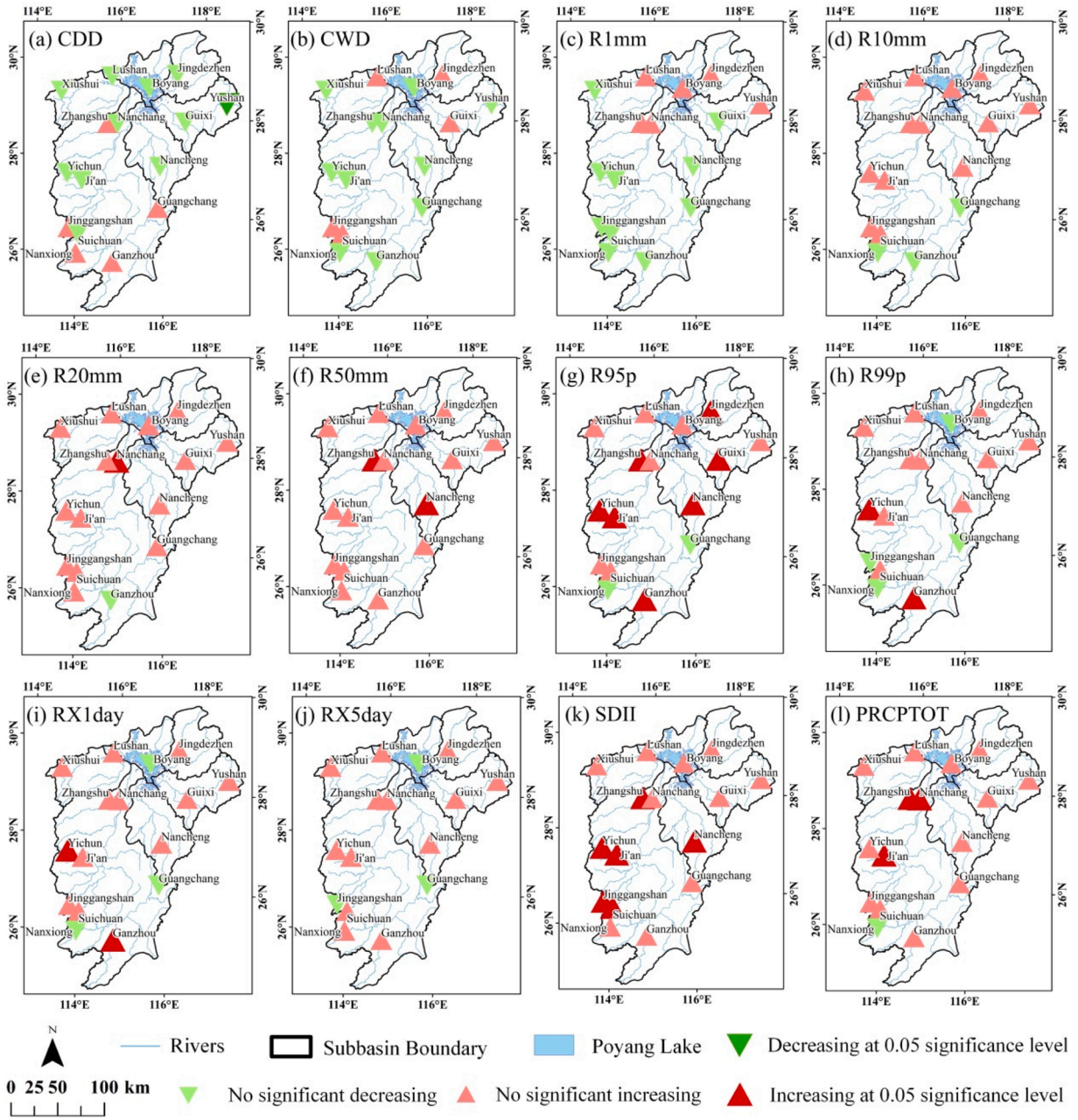

Fig. 4. Spatial distribution of the PWMK test for 12 extreme precipitation indices in PLB during 1959–2019.

3.3. Risk changes of extreme precipitation

For the different index types, CWD, R50 mm, RX1day, and RX5day were selected to represent the duration, frequency, and intensity, respectively. The extreme precipitation amounts at 20-, 100-, and 500-yr return periods by GAMLSS were applied to analyze the risk of extreme precipitation for each station from 1959 to 2019. Fig. 8 shows that the northeastern and southwestern parts of the PLB had longer rainfall durations, but the trends reversed, with the northeastern part showing a decreasing trend and the southwestern part showing an increasing trend. Nanchang in the central part of the PLB showed a shorter duration and a decreasing trend. Overall, CWD increased as the return period increases. In terms of the different return periods, the maximum rainfall duration increased by four days from the 20-yr to the 100-yr and by two days from the 100-yr to the 500-yr return period. The range of low-value centers gradually decreased, with the smallest range observed in the 100-yr return period.

Fig. 9 shows a significant increasing trend at all stations except for Zhangshu, Nanchang, Yushan, and Jinggangshan. In general, the number of rainstorms increased from southwest to the northeast. Among them, Yushan was heavy rainfall center, while Nanxiong was

Table 5
Statistics of PWMK trend for extreme precipitation indices at the stations.

No.	Station	Significant increasing	Increasing	No trend	Decreasing	Significant decreasing
1	Xiushui	0	9	0	3	0
2	Yichun	4	5	0	3	0
3	Ji'an	3	6	0	3	0
4	Jinggangshan	1	8	1	2	0
5	Suichuan	1	8	1	2	0
6	Ganzhou	3	4	1	4	0
7	Nanxiong	0	5	1	6	0
8	Lushan	0	9	2	1	0
9	Boyang	0	7	0	5	0
10	Jingdezhen	1	10	0	1	0
11	Nanchang	2	8	0	2	0
12	Zhangshu	4	7	0	1	0
13	Guixi	1	8	1	2	0
14	Yushan	0	10	0	1	1
15	Nancheng	3	6	0	3	0
16	Guangchang	0	5	2	5	0

Table 6
Statistics of PWMK trends for stations with respect to the extreme precipitation indices.

No.	Indices	Significant increasing	Increasing	No trend	Decreasing	Significant decreasing
1	CDD	0	5	0	10	1
2	CWD	0	2	3	11	0
3	R1mm	0	5	1	10	0
4	R10mm	0	13	0	3	0
5	R20mm	1	14	0	1	0
6	R50mm	2	14	0	0	0
7	R95p	7	7	1	1	0
8	R99p	2	10	3	1	0
9	RX1day	2	11	0	3	0
10	RX5day	0	13	0	3	0
11	SDII	6	10	0	0	0
12	PRCPTOT	3	11	1	1	0

the low rainfall center. In terms of the different return periods, the maximum number of rainstorms increased by six days from the 20-yr to the 100-yr return period, and by three days from the 100-yr to the 500-yr return period. Additionally, the frequency of heavy rainfall at Yushan with a 500-yr event was twice that of Nanxiong.

The results of the three return periods for RX1day (Fig. 10) showed that the southwestern part of the basin was the center of low values and the southeastern and northwestern parts were the centers of high values. Additionally, most of the stations in the PLB showed a significant increasing trend. In terms of the different return periods, the maximum number of RX1day increased by 50 mm from the 20-yr to the 500-yr return period.

RX5day reflects the intensity and duration of the extreme precipitation. Fig. 11 indicates that Lushan in the northwestern and Guixi in the northeastern part of the PLB were the high-value centers of RX5day, while the southwestern part was the low-value center of RX5day. The low-value centers in the southwestern region showed an increasing trend, whereas the high-value centers in the north showed a decreasing trend. As the return period increased, the rank of Nancheng decreased and that of Guangchang increased.

To more intuitively illustrate the recurrence risk of extreme precipitation, three stations with significant non-stationary characteristics were selected: Jingdezhen, Nanchang, and Ganzhou located in the upper, middle, and lower PLB, respectively. Additionally, we compared the RX1day, R50 mm, and CWD variation under stationary (no trend in Mn and Var) and non-stationary (the result of the GAMLSS model) conditions for different return periods. For RX1day, Jingdezhen is Mn non-stationarity, Nanchang is Mn and Var non-stationarity, and Ganzhou is Var non-stationarity. For R50 mm and CWD, Nanchang is Var non-stationarity and Mn non-stationarity, respectively. The non-stationarity model was able to better capture the trend in RX1day over time and better fit the trend change characteristics in the very high and very low value years than the stationary model (Fig. 12). It can be seen that the non-stationary model is better for assessing the recurrence risk of the intensity, frequency, and duration of extreme precipitation events.

From a different station perspective, Jingdezhen under stationary conditions exceeded the 500-yr return period in both 2012 and 2018, while under non-stationary conditions, the year 2012 was placed between the 100-yr and 500-yr return periods (Fig. 12a). The return period for non-stationary conditions at Jingdezhen continued to increase between 1959 and 1970. The highest RX1day under the 500-yr return period occurred in 1970 and then decreased slightly. However, the growth continued after 1990 and has increased in recent years, reaching 503.16 mm in 2019.

Nanchang, the capital of Jiangxi Province, the intensity, frequency, and duration of extreme precipitation showed non-stationary characteristics. For the RX1day, Nanchang showed a bimodal variation characteristic of non-stationary conditions, with peaks of 306.63 and 473.54 mm around 1973 and 2001 for the 500-yr return period, respectively, and a significant downward trend after 2001

Table 7
Distribution characteristics and lineaments of the extreme precipitation indices at stations.

No.	CDD	CWD	R1mm	R10mm	R20mm	R50mm	R95p	R99p	RX1day	RX5day	SDII	PRCPTOT
1	IGAMMA-1	RG-7*	NO-4*	IG-2	GA-8*	GA-1	GA-2	RG-1	IGAMMA-1	IGAMMA-2	RG-1	RG-2
2	IGAMMA-2	RG-2	LO-2	NO-1	GA-1	RG-1	WEI3-1	RG-5	IGAMMA-1	IGAMMA-1	IG-7*	NO-1
3	IGAMMA-3*	RG-8*	NO-3*	GA-1	WEI3-1	NO-1	WEI3-3*	RG-6*	IGAMMA-1	RG-4*	GA-1	GA-1
4	RG-3*	RG-2	LO-3*	GA-2	NO-7*	GA-2	GA-4*	RG-2	IG-2	IGAMMA-3*	LO-7*	GA-7*
5	IG-4*	IGAMMA-4*	IGAMMA-3*	NO-2	NO-1	RG-3*	RG-1	RG-2	IG-2	IG-3*	LO-1	GA-1
6	IGAMMA-2	IGAMMA-3*	RG-1	IG-2	GA-2	GA-1	GA-1	RG-1	IGAMMA-7*	RG-1	IG-1	IGAMMA-2
7	GA-1	RG-3*	IGAMMA-2	IGAMMA-2	NO-2	NO-2	NO-1	RG-1	GA-2	GA-2	GA-2	IG-2
8	IGAMMA-3*	RG-2	WEI3-1	NO-7*	WEI3-3*	WEI3-1	WEI3-1	RG-2	IG-1	IGAMMA-4*	LOGNO-1	GA-7*
9	IG-4*	LOGNO-2	NO-8*	GA-7*	IG-1	GA-1	RG-1	RG-1	IGAMMA-1	RG-4*	RG-1	IG-7*
10	RG-1	IG-2	NO-1	GA-3*	IG-1	GA-1	WEI3-1	RG-2	IGAMMA-3*	IG-3*	IGAMMA-1	GA-1
11	IGAMMA-1	GA-3*	NO-3*	IG-1	IG-7*	GA-4*	GA-4*	RG-3*	IGAMMA-8*	IGAMMA-1	RG-4*	RG-7*
12	IG-7*	IG-3*	NO-4*	NO-1	GA-1	NO-7*	WEI3-3*	RG-2	RG-2	IG-2	NO-1	WEI3-1
13	IGAMMA-2	IG-2	WEI3-2	GA-1	IG-1	WEI3-1	RG-1	RG-2	IG-1	IG-2	IGAMMA-1	GA-1
14	IGAMMA-1	IGAMMA-1	WEI3-2	GA-1	IG-1	GA-2	WEI3-2	RG-2	IG-1	IGAMMA-3*	RG-1	IG-1
15	GA-4*	IGAMMA-5	NO-2	NO-1	NO-1	RG-5	RG-5	RG-6*	IGAMMA-7*	IG-1	NO-5	LO-5
16	IGAMMA-2	RG-1	GA-1	GA-2	NO-2	WEI3-1	WEI3-1	RG-2	IGAMMA-4*	IGAMMA-4*	RG-1	IG-2

Notes: * represents non-stationarity; the serial numbers of the stations are listed in Table 5, the same blow; the abbreviations of distribution functions and line types are listed in Table 2 and Table 3, respectively.

Table 8
Statistics of GAMLSS model for extreme precipitation indices at station.

No.	Station	Number of stationary	Number of non-stationary	Optimal distribution	Optimal linearity
1	Xiushui	9	3	IGAMMA	1
2	Yichun	11	1	IGAMMA	1
3	Ji'an	6	6	RG	1
4	Jinggangshan	5	7	RG	2
5	Suichuan	7	5	IG	1
6	Ganzhou	10	2	IGAMMA	1
7	Nanxiong	11	1	GA	2
8	Lushan	7	5	WEI3	1
9	Boyang	7	5	RG	1
10	Jingdezhen	9	3	IG	1
11	Nanchang	3	9	IGAMMA	1
12	Zhangshu	7	5	NO	1
13	Guixi	12	0	IG	1
14	Yushan	11	1	IGAMMA	1
15	Nancheng	9	3	NO	5
16	Guangchang	10	2	IGAMMA	2

Table 9
Statistics of the GAMLSS model for stations with respect to extreme precipitation indices.

No.	Indices	Number of stationary	Number of non-stationary	Optimal distribution	Optimal linearity
1	CDD	9	7	IGAMMA	1
2	CWD	9	7	RG	2
3	R1mm	9	7	NO	2
4	R10mm	13	3	GA	1
5	R20mm	12	4	NO	1
6	R50mm	13	3	GA	1
7	R95p	12	4	WEI3	1
8	R99p	13	3	RG	2
9	RX1day	11	5	IGAMMA	1
10	RX5day	8	8	IGAMMA	2
11	SDII	13	3	RG	1
12	PRCPTOT	12	4	GA	1

(Fig. 12b). For R50 mm, the highest value of 13 d occurred in 1959, and the lowest value of 1 d occurred in 2007 (Fig. 12d). The frequency of extreme precipitation in Nanchang shows greater fluctuations owing to Var non-stationarity. In terms of CWD, the return period of extreme precipitation duration in Nanchang increased with time, showing a linear trend (Fig. 12e). There was a great difference in the performance of the stationary and non-stationary conditions. The former had a lower value than the latter under the same return period.

Ganzhou shows an "L" shaped trend under non-stationary conditions, with the highest value of 342.41 mm occurring in 1959 and the lowest value of 125.25 mm in 1971 (Fig. 12c). Under non-stationary conditions, RX1day reached the 100-yr and 20-yr return period levels in 1961 and 1982, respectively. However, under stationary conditions, 1961 exceeded the 500-yr return period. Furthermore, from 1967 to 1977, the 500-yr return period under non-stationary conditions was lower than the 20-yr return period under stationary conditions.

In general, the Mn non-stationarity and Var non-stationarity caused trend changes and fluctuating changes in the return period, respectively. If both Mn and Var show non-stationary characteristics, then the variation of extreme precipitation return period will be more obvious and bring a higher risk of disaster. For example, the results of the return periods of intensity, frequency, and duration of extreme precipitation events in Nanchang indicated that non-stationarity was more likely to change the return periods of extreme precipitation intensity than frequency and duration.

The values for the stationary and non-stationary characteristics differed significantly across time (Table 10), with higher values for the non-stationary model overall. Furthermore, the difference between the non-stationary and stationary models became more significant as time increased, particularly after 1985. In the 20-yr return period of RX1day, the stationary model showed higher values from 1959 to 1984. In contrast, in the 100-yr return period of RX1day, the non-stationary model was higher than the stationary model after 1970. The overall value of the non-stationary model was higher than that of the stationary model for the 500-yr return period of RX1day.

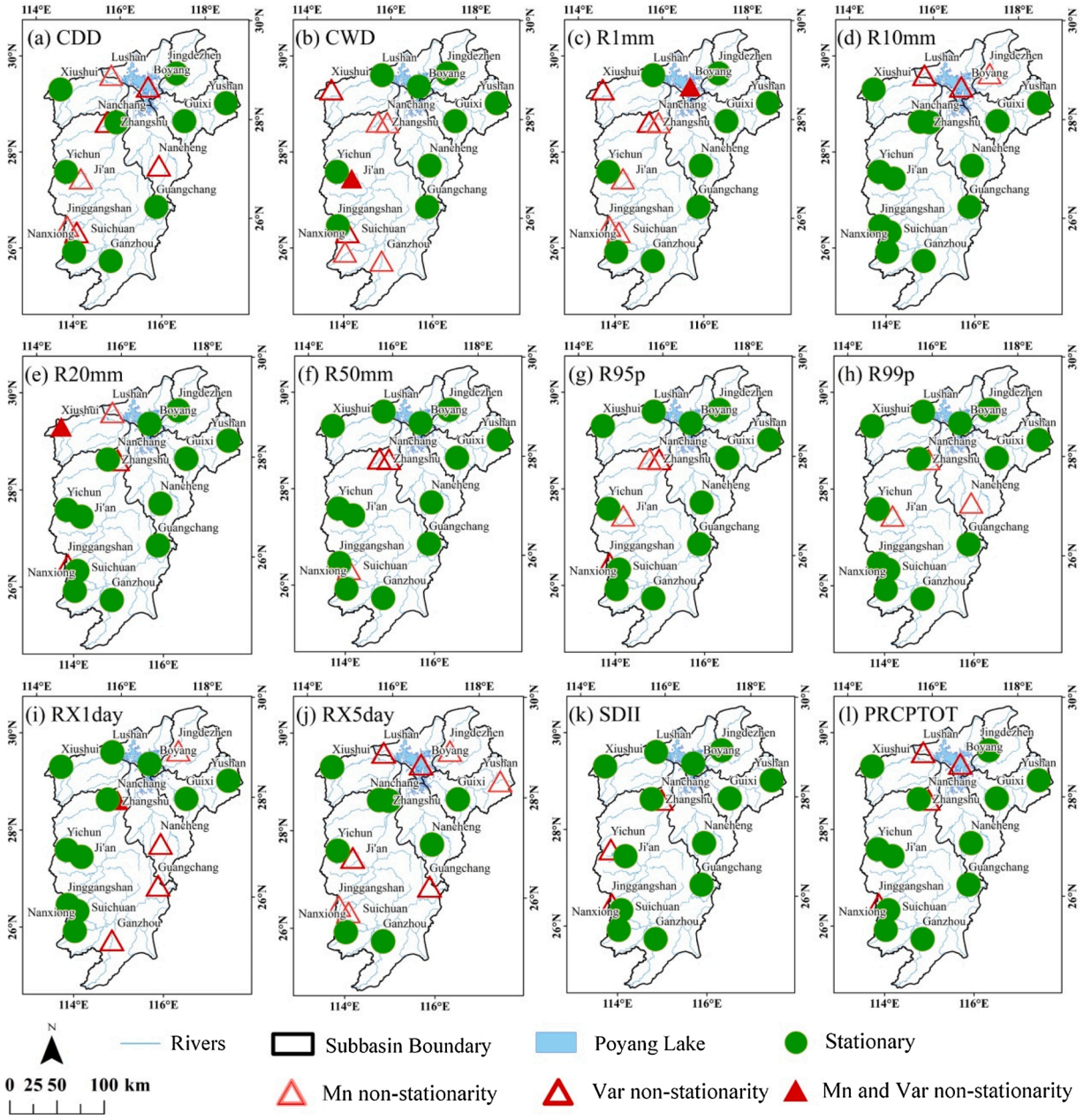

Fig. 5. Spatial distribution of the GAMLSS model for extreme precipitation indices in PLB.

4. Discussion

4.1. Spatio-temporal variation in extreme precipitation

The results show that the intensity and frequency of extreme precipitation increased significantly during the past 61 years in the PLB, whereas the duration of extreme precipitation decreased significantly. Zhang et al. (2015) also found that the intensity of moderate and heavy rainfall increased in the PLB. Moreover, the annual area affected by extreme precipitation events showed a general upward trend of 400 km^2/year (Zhan et al., 2019). Fig. 2 shows that 1990–2000 and 2010–2015 had a high occurrence of extreme precipitation events. In 1990–2000, increased rainfall due to ENSO caused severe flooding in the PLB in 1992, 1995, and 1998 (Hu et al., 2007; Shankman et al., 2006). In 2010–2015, the PLB experienced severe drought events in 2012, 2013, and 2015. These results indicate that there is an unequal temporal distribution of precipitation in the PLB. Extreme precipitation events concentrated in the flood season (April–September) can not only lead to flooding, but also to drought events in the non-flood season (October–March).

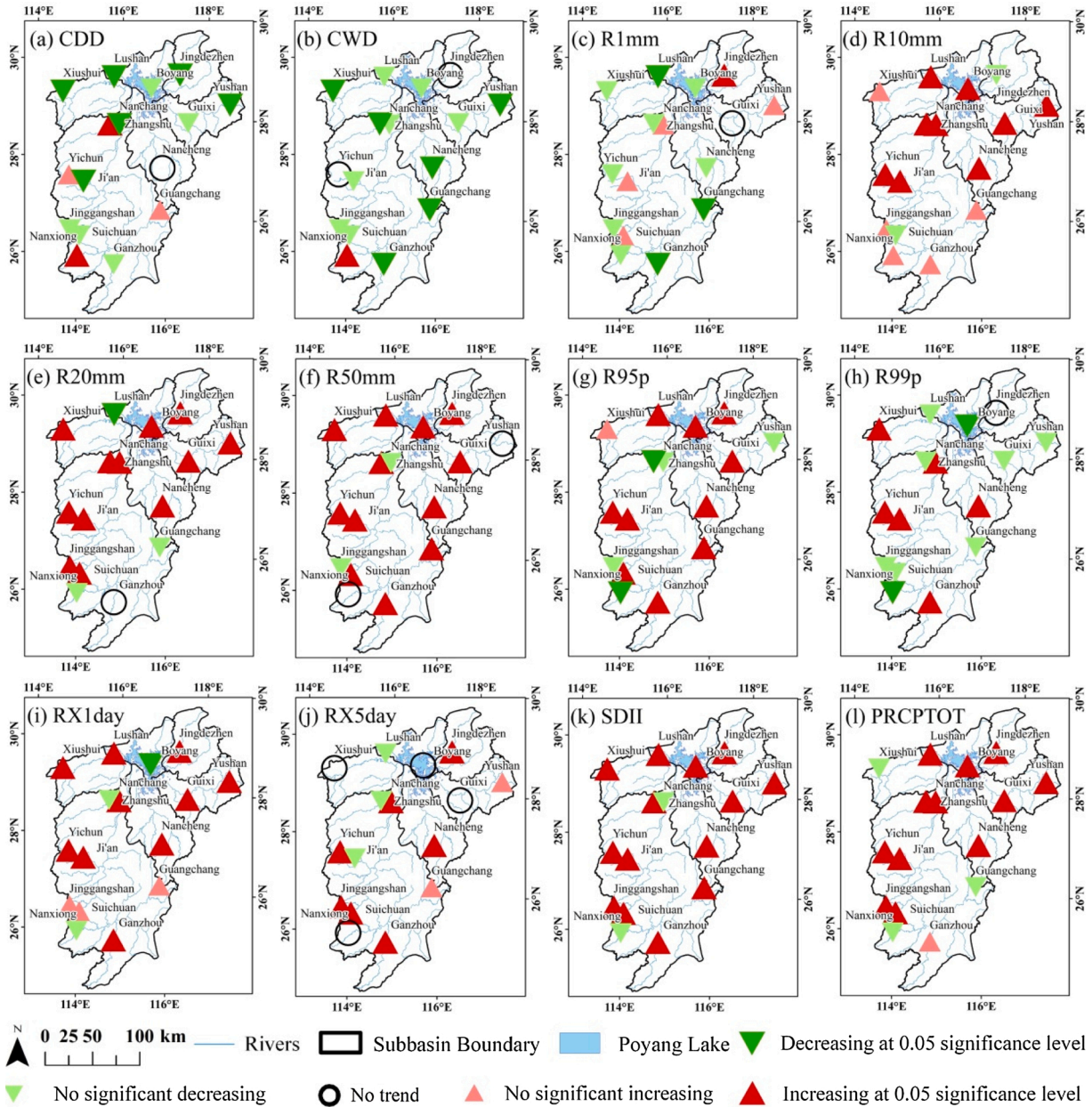

Fig. 6. Spatial distribution of PWMK test for Mn of extreme precipitation indices from 1959 to 2019.

In general, Var is an important indicator of non-stationarity. Variations in Var imply an increase and decrease in precipitation, which leads to floods and droughts, respectively. The non-stationary characteristics of precipitation in the PLB were further verified by drought and flood in 2019 and 2020, respectively. The runoff in the PLB increases during the flood season due to precipitation increases and the interaction between the Yangtze River flow and PLB (Hu et al., 2007). Therefore, extreme precipitation during the flood season is often associated with floods (Tang et al., 2021; Zhou et al., 2021). Moreover, extreme precipitation during the non-flood season is the main cause of runoff variation (Lei et al., 2021). Drought events are likely to occur once precipitation is lower than the mean climatology (Lu et al., 2021). Additionally, in terms of geospatial distribution, extreme precipitation trends increased significantly in the southwestern, eastern, and northeastern areas of the PLB. Li and Hu (2019) reported that the northeastern and eastern areas experienced a higher frequency of extreme precipitation events. This is due to the fact that extreme precipitation tends to occur during the flood season. Topography at high altitudes during summer and autumn is conducive to the formation of extreme precipitation conditions (Zhang et al., 2014). Therefore, there is a significant trend of increasing extreme precipitation in the south and east. Furthermore, high-altitude topography in different regions contributes positively to extreme precipitation (Guan et al., 2017).

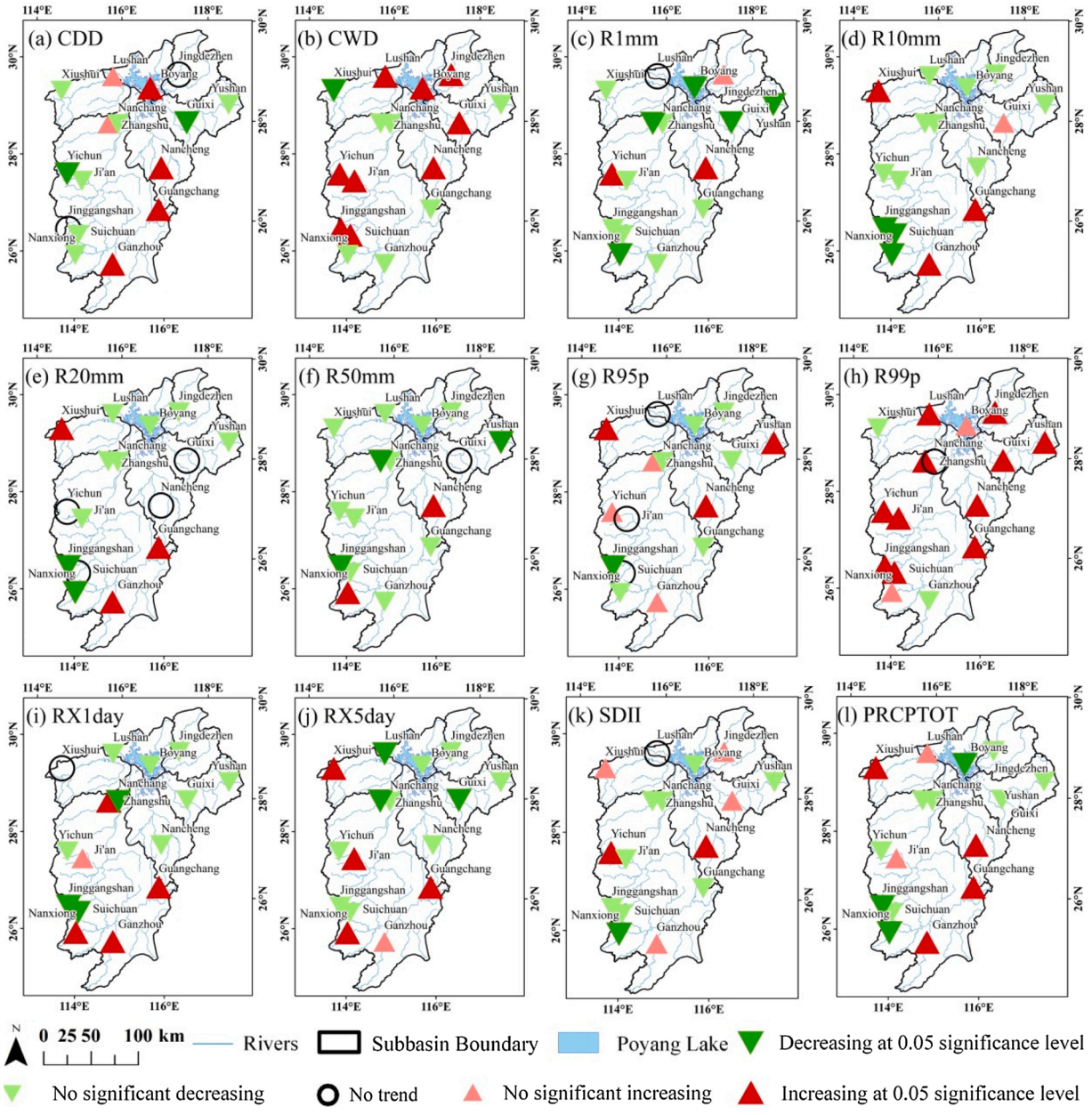

Fig. 7. Spatial distribution of the PWMK test for Var of the extreme precipitation indices from 1959 to 2019.

4.2. Non-stationary characteristics of extreme precipitation indices

The GAMLSS model results, shown in Tables 7–9, indicate that the extreme precipitation indices in the PLB are dominated by stationary characteristics. However, the Nanchang site exhibited significant non-stationary characteristics and showed a significant trend of increasing intensity and frequency of extreme precipitation events over the past 61 years. In fact, frequent climate change and human activities in recent years have affected the stationary characteristics of extreme precipitation in the PLB. In terms of the impact of climate change, precipitation in the PLB is influenced by several atmospheric circulation indices (Xiao et al., 2015; Zhu et al., 2020). Human activities have increased daily precipitation extremes by approximately 13 % (Chen and Sun, 2017). Moreover, as urbanization increases, land use changes affect the global and local climate by changing the atmospheric moisture and ecological balance (Salazar et al., 2015). Nanchang is the economic, political, and cultural center of the Jiangxi Province. With the accelerating urbanization since the 1978 economic reforms, human activities in Nanchang have become increasingly frequent (Wang, 2020). Meanwhile, increased CO_2 emissions, reduced vegetation cover, and large amounts of reclaimed agricultural land (Li et al., 2012) have contributed to local climate change. Gao et al. (2018) found that climate indices can affect mean-state Var during extreme precipitation events, and human

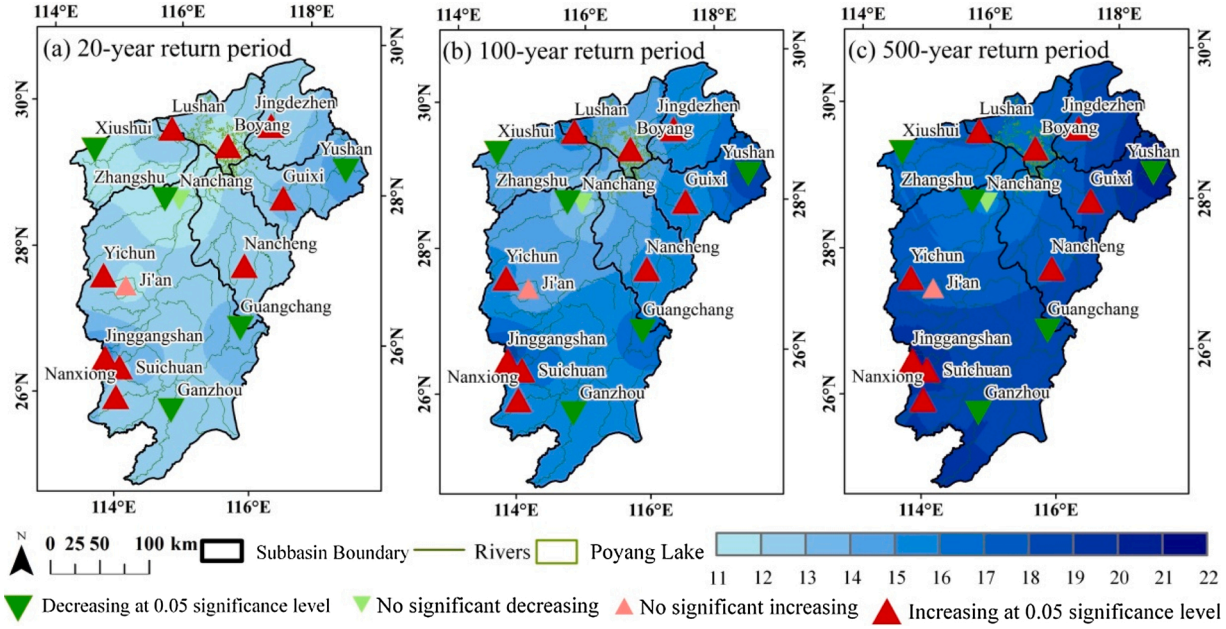

Fig. 8. Spatial distribution of CWD (d) for 20-, 100-, and 500-yr return periods as well as the PWMK trends.

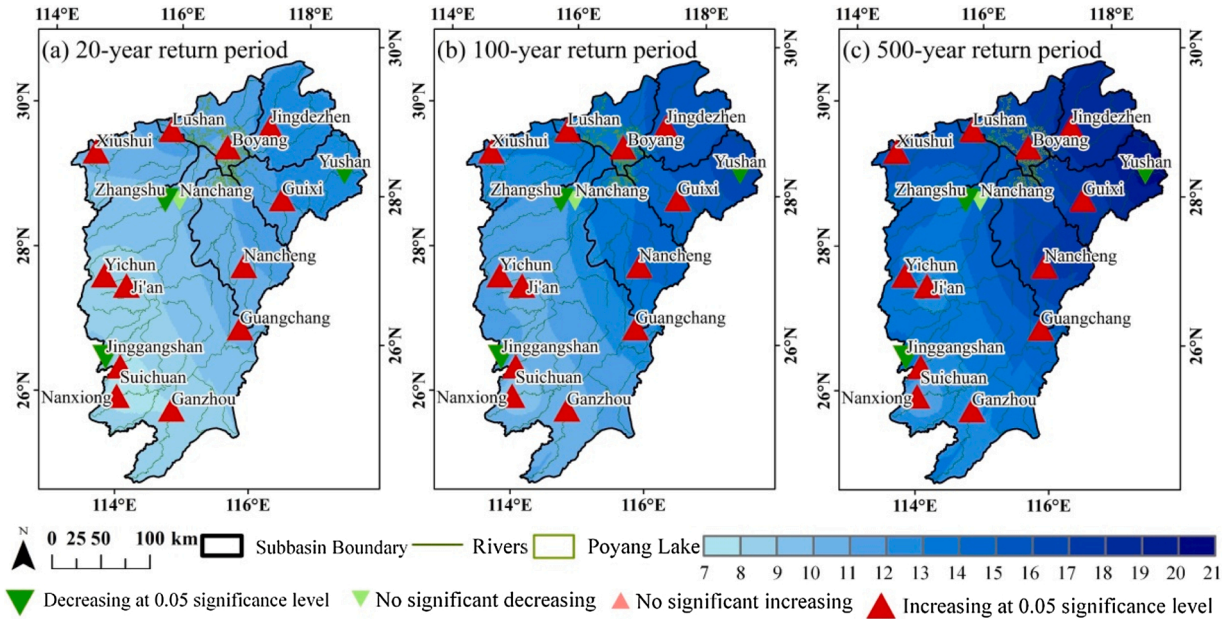

Fig. 9. Spatial distribution of R50 mm (d) for the 20-, 100-, and 500-yr return periods as well as the PWMK trends.

activities can lead to significant changes in extreme precipitation events. Therefore, the non-stationary characteristics of Nanchang are mainly caused by frequent human activities. At the same time, the results of the trend test for Var (Fig. 7) show relatively less stability for the stations at higher altitudes and an increasing trend, which indicates that topography has an influence on extreme precipitation events.

4.3. Risk changes of extreme precipitation

Previous studies have shown that GAMLSS is suitable for assessing the non-stationary characteristics of extreme precipitation indices and their attributes (Gao et al., 2018; Zhang et al., 2015, 2014). It can also be used to calculate extreme precipitation amounts

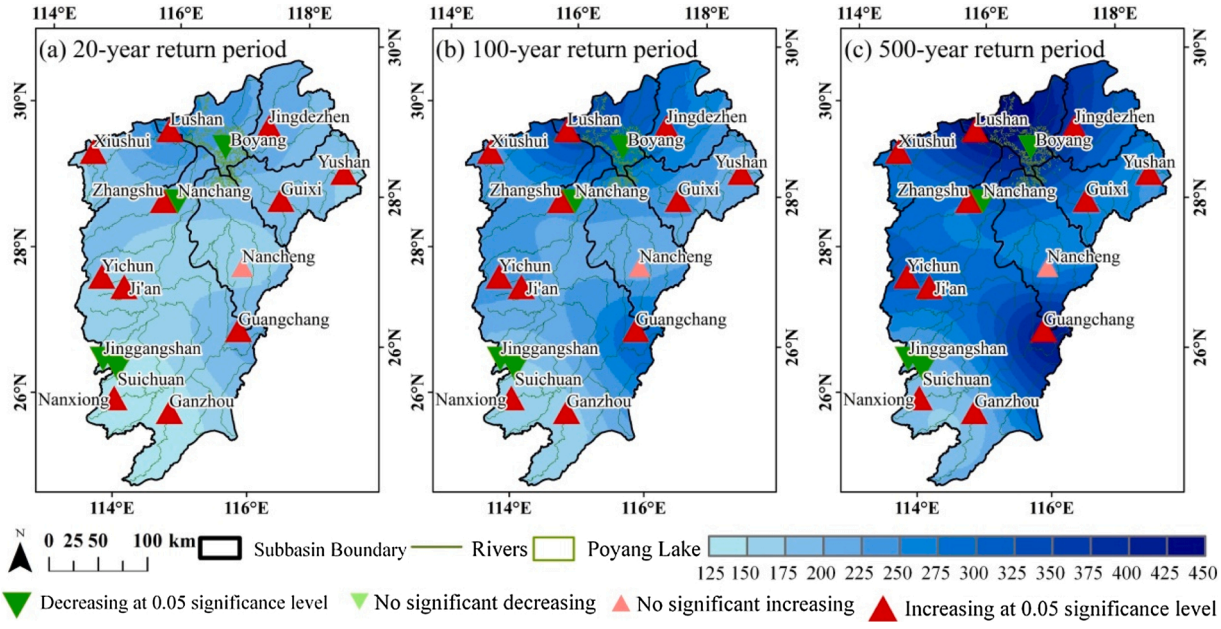

Fig. 10. Spatial distribution of RX1day (mm) for the 20-, 100-, and 500-yr return periods as well as the PWMK trends.

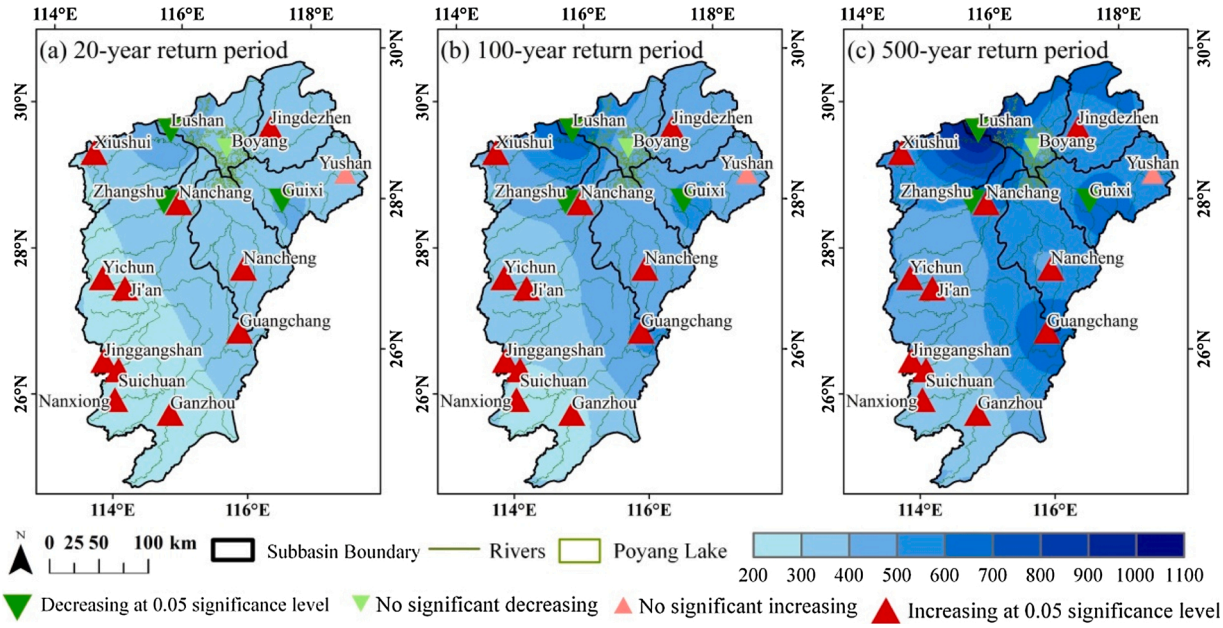

Fig. 11. Spatial distribution of RX5day (mm) for 20-, 100-, and 500-yr return periods as well as the PWMK trends.

at different return periods (Gao et al., 2017). Figs. 8–11 show that the high value of extreme precipitation events in the basin is located in the north and east, and the low values are located in the southwest. Moreover, the higher elevations in the east and south, which are more mountainous and hilly landscapes, make the local climate susceptible to the effects of elevation. Most areas of the PLB are below the medium level in the 20-yr return period of each index, particularly in the plains.

However, comparing the variation of RX1day over time for different stations (Fig. 12a–c) showed that Jingdezhen and Nanchang have higher values than Ganzhou in both the stationary and non-stationary models. Previous studies have shown that the EASM significantly contributes to precipitation in the middle and lower reaches of the Yangtze River, particularly in summer (Ren et al., 2013; Xiao et al., 2015; Zhu et al., 2020). Jingdezhen and Nanchang are closer to Poyang Lake and the Yangtze River than Ganzhou and are thus more susceptible to changes in water moisture. Hence, the values of the extreme precipitation events were high. With extreme precipitation events showing non-stationary characteristics, we need to be aware that there is a possibility of future flooding in

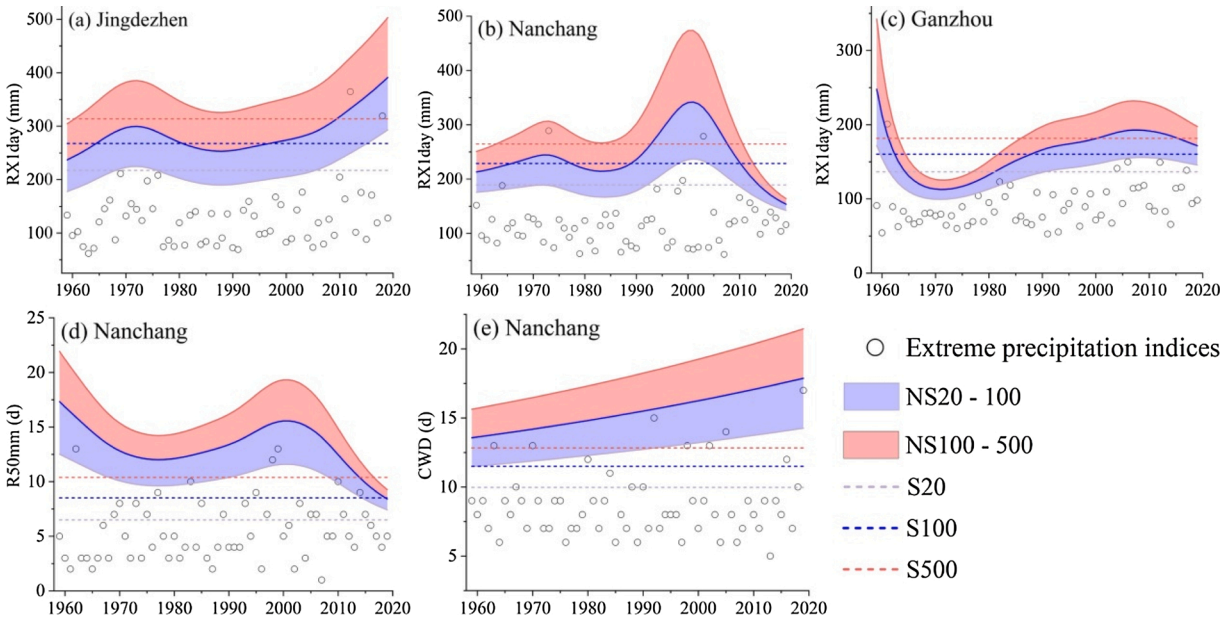

Fig. 12. Comparison of stationary (S) and non-stationary (NS) characteristics of extreme precipitation indices under the three return periods at typical stations (upper, middle, and lower) in the PLB. (a) RX1day at Jingdezhen; (b) RX1day at Nanchang; (c) RX1day at Ganzhou; (d) R50 mm at Nanchang; (e) CWD at Nanchang.

Table 10
Differences in the values of RX1day for typical stations under non-stationary conditions at different time periods for the 20, 100, 500-yr return periods compared to the stationary conditions.

Station	1959–1969	1970–1984	1985–1999	2000–2019
Jingdezhen	−18.3 / −2.5 / **27.5**	−6 / **13.9** / **48.6**	−22.2 / −7.8 / **20.7**	**23.4** / **53.1** / **98.9**
Nanchang	−8.4 / −4.4 / **5.8**	−11.2 / **0.8** / **22.0**	**4.4** / **35.3** / **83.1**	**2.1** / **16.5** / **42.9**
Ganzhou	−13.5 / −5.0 / **9.8**	−28.2 / −35.1 / −39.8	**0.8** / **7.7** / **18.3**	**15.4** / **25.5** / **39.5**

Note: bold values indicate higher values for non-stationary conditions than for the stationary conditions.

Nanchang. In addition, the results in Fig. 12 show that the non-stationary model can be unusually low in individual years, such as in Nanchang from 2016 to 2019 and Ganzhou from 1967 to 1977. Therefore, the design of rainfall flood protection standards should integrate stationary and non-stationary models to avoid excessive fluctuations in standards.

In general, Mn non-stationarity and Var non-stationarity changed the trend and fluctuation state of the return period of extreme precipitation events, respectively. The combination of the two can have a significant impact on extreme precipitation events.

5. Conclusion

In this study, 12 extreme precipitation indices were selected to analyze the spatial and temporal variations of extreme precipitation in the PLB based on the PWMK and GAMLSS models. The variation in the return period under non-stationary conditions was also investigated. The results provide a scientific basis for water resource management and disaster prevention in the PLB. The important conclusions drawn from this study are as follows.

(1) Extreme precipitation intensities and frequency in the PLB increased from 1959 to 2019, while the duration of extreme precipitation decreased significantly. For instance, R50 mm increased by 0.43 days and CWD decreased by 1.58 days. R95p increased by 141.33 mm, which accounted for more than 87 % of PRCPTOT. Additionally, extreme precipitation trends increased significantly in the southwestern, eastern, and northeastern areas of the PLB. The number of extreme precipitation indices that showed an increase at the Jingdezhen site was twice that at the Nanxiong site.
(2) Most of the extreme precipitation indices showed stationary characteristics in most parts of the PLB. The duration of extreme precipitation showed significant non-stationary characteristics in the western PLB. However, at the site scale, stationary and non-stationary characteristics appeared separately with respect to different indices, particularly for Nanchang, with 83.3 % of extreme precipitation intensity indices showing non-stationary characteristics.
(3) The trend of the Mn of the extreme precipitation indices increased more than Var. However, the Mn of extreme precipitation duration showed a significant decrease, while Var showed an increasing trend.

(4) The risk of extreme precipitation increased significantly for different return periods under non-stationary conditions in the northwest and northeast of the PLB. The duration and frequency of extreme precipitation increased from southwest to northeast. The intensity of extreme precipitation was higher in the southeastern and northwestern parts of the PLB. The RX1day and RX5day in the northwestern part of the PLB were twice that of the southwestern PLB under the 500-yr return period.
(5) The risk of extreme precipitation in the PLB could be better captured and simulated using a non-stationary model. The risk of extreme precipitation in most parts of the PLB was below the medium level in the 20-yr return period, particularly in the plains. In the last 10 years, the stationary method has significantly underestimated the extreme precipitation intensity at the Jingdezhen and Ganzhou sites for the 500-yr return period. There is also an underestimation of the frequency and duration of the return period of extreme precipitation events. In the future, more attention should be paid to the increase and fluctuation of the return period of extreme precipitation events caused by Mn non-stationarity and Var non-stationarity, as well as the extreme precipitation events caused by the combination of the two.

Author statement

L.G. and X. L. designed the research and collected the data, X. L., L. W. and H. L. contributed to the data processing and analysis, X. L. prepared the original draft, L. G. edited and reviewed the manuscript, M. M., L. X. and J. W. contributed to the discussion. All authors have read and agreed to the published version of the manuscript.

Declaration of Competing Interest

The authors declare that there are no conflicts of interest in this paper.

Acknowledgments

This work was supported by the National Key Research and Development Program of China (2018YFE0206400), the Scientific Project from Fujian Provincial Department of Science and Technology (2019R1002-3), the Scientific Project from Fujian Key Laboratory of Severe Weather (2020KFKT01) and the Outstanding Young Scientific Research Talents Cultivation Program, Education Department of Fujian Province. Dr. Jianhui Wei was supported financially by the German Research Foundation through funding of the AccHydro project (DFG-Grant KU 2090/11-1). The meteorological data have been provided the China Meteorological Data Sharing Service System of National Meteorological Information Center (http://data.cma.cn/).

Appendix A. Supplementary data

Supplementary material related to this article can be found, in the online version, at doi:https://doi.org/10.1016/j.ejrh.2021.100920.

References

Alexander, L.V., 2016. Global observed long-term changes in temperature and precipitation extremes: a review of progress and limitations in IPCC assessments and beyond. Weather. Clim. Extremes. 11, 4–16. https://doi.org/10.1016/j.wace.2015.10.007.
Alexander, L.V., Fowler, H.J., Bador, M., Behrangi, A., Donat, M.G., Dunn, R., Funk, C., Goldie, J., Lewis, E., Roge, M., Seneviratne, S.I., Vengupal, V., 2019. On the use of indices to study extreme precipitation on sub-daily and daily timescales. Environ. Res. Lett. 14, 125008 https://doi.org/10.1088/1748-9326/ab51b6.
Ali, H., Fowler, H.J., Mishra, V., 2018. Global observational evidence of strong linkage between dew point temperature and precipitation extremes. Geophys. Res. Lett. 45, 12320–12330. https://doi.org/10.1029/2018gl080557.
Chen, H.P., Sun, J.Q., 2017. Contribution of human influence to increased daily precipitation extremes over China. Geophys. Res. Lett. 44, 2436–2444. https://doi.org/10.1002/2016gl072439.
Chen, M.Z., Papadikis, K., Jun, C.Y., 2021. An investigation on the non-stationarity of flood frequency across the UK. J. Hydrol. 597, 126309 https://doi.org/10.1016/j.jhydrol.2021.126309.
Croitoru, A.E., Chiotoroiu, B.C., Ivanova Todorova, V., Torică, V., 2013. Changes in precipitation extremes on the Black Sea Western Coast. Glob. Planet. Change 102, 10–19. https://doi.org/10.1016/j.gloplacha.2013.01.004.
Das, S., Scaringi, G., 2021. River flooding in a changing climate: rainfall-discharge trends, controlling factors, and susceptibility mapping for the Mahi catchment, Western India. Nat. Hazards. https://doi.org/10.1007/s11069-021-04927-y.
Gao, L., Huang, J., Chen, X.W., Chen, Y., Liu, M.B., 2017. Risk of extreme precipitation under nonstationarity conditions during the second flood season in the Southeastern Coastal Region of China. J. Hydrometeorol. 18 (3), 669–681. https://doi.org/10.1175/JHM-D-16-0119.1.
Gao, L., Huang, J., Chen, X.W., Chen, Y., Liu, M.B., 2018. Contributions of natural climate changes and human activities to the trend of extreme precipitation. Atmos. Res. 205, 60–69. https://doi.org/10.1016/j.atmosres.2018.02.006.
Gao, X.C., Guo, M., Yang, Z.Y., Zhu, Q., Xu, Z., Gao, K., 2020. Temperature dependence of extreme precipitation over mainland China. J. Hydrol. 583, 124595 https://doi.org/10.1016/j.jhydrol.2020.124595.
Guan, Y.H., Zheng, F.L., Zhang, X.C., Wang, B., 2017. Trends and variability of daily precipitation and extremes during 1960-2012 in the Yangtze River Basin, China. Int. J. Climatol. 37, 1282–1298. https://doi.org/10.1002/joc.4776.
Gudmundsson, L., Boulange, J., Do, H.X., Gosling, S.N., Grillakis, M.G., Koutroulis, A.G., Leonard, M., Liu, J., Muller Schmied, H., Papadimitriou, L., Pokhrel, Y., Seneviratne, S.I., Satoh, Y., Thiery, W., Westra, S., Zhang, X.B., Zhao, F., 2021. Globally observed trends in mean and extreme river flow attributed to climate change. Science 371, 1159–1162. https://doi.org/10.1126/science.aba3996.
Hu, Q., Feng, S., Guo, H., Chen, G.Y., Jiang, T., 2007. Interactions of the Yangtze river flow and hydrologic processes of the Poyang Lake, China. J. Hydrol. 347, 90–100. https://doi.org/10.1016/j.jhydrol.2007.09.005.

Ingram, W., 2016. Extreme precipitation: increases all round. Nat. Clim. Chang. 6, 443–444. https://doi.org/10.1038/nclimate2966.
IPCC, 2014. Climate Change 2014: Impacts, Adaptation and Vulnerability: Part A: Global and Sectoral Aspects. Cambridge University Press, Cambridge. https://doi.org/10.1017/CBO9781107415379.
Kendall, M.G., 1975. Rank Correlation Methods, Fourth ed. Charles Griffin, London.
Khan, N., Shahid, S., Chung, E.S., Behlil, F., Darwish, M.S.J., 2020. Spatiotemporal changes in precipitation extremes in the arid province of Pakistan with removal of the influence of natural climate variability. Theor. Appl. Climatol. 142, 1447–1462. https://doi.org/10.1007/s00704-020-03389-9.
Kundzewicz, Z.W., Huang, J.L., Pinskwar, I., Su, B., Szwed, M., Jiang, T., 2020. Climate variability and floods in China - A review. Earth-Sci. Rev. 211, 103434 https://doi.org/10.1016/j.earscirev.2020.103434.
Lei, X.Y., Gao, L., Wei, J.H., Ma, M.M., Xu, L.G., Fan, H.X., Li, X.H., Gao, J.Y., Dang, H.F., Chen, X.W., Fang, W.H., 2021. Contributions of climate change and human activities to runoff variations in the Poyang Lake Basin of China. Phys. Chem. Earth, Parts B 123, 103019. https://doi.org/10.1016/j.pce.2021.103019.
Li, W., Chen, Y., 2021. Detectability of the trend in precipitation characteristics over China from 1961 to 2017. Int. J. Climatol. 41, E1980–E1991. https://doi.org/10.1002/joc.6826.
Li, X.H., Hu, Q., 2019. Spatiotemporal changes in extreme precipitation and its dependence on topography over the Poyang Lake Basin, China. Adv. Meteorol. 22, 1–15. https://doi.org/10.1155/2019/1253932.
Li, P., Feng, Z.M., Jiang, L.G., Liu, Y.J., Xiao, X.M., 2012. Changes in rice cropping systems in the Poyang Lake Region, China during 2004–2010. J. Geogr. Sci. 22, 653–668. https://doi.org/10.1007/s11442-012-0954-x.
Li, X.H., Hu, Q., Wang, R., Zhang, D., Zhang, Q., 2021. Influences of the timing of extreme precipitation on floods in Poyang Lake, China. Hydrol. Res. 52 (1), 26–42. https://doi.org/10.2166/nh.2021.078.
Lu, F., Song, X.Y., Xiao, W.H., Zhu, K., Xie, Z.B., 2020. Detecting the impact of climate and reservoirs on extreme floods using nonstationary frequency models. Stoch. Environ. Res. Risk Assess. 34, 1–14. https://doi.org/10.1007/s00477-019-01747-2.
Lu, C.H., Jiang, J., Chen, R.D., Ullah, S., Yu, R., Lott, F.C., Tett, S.F.B., Dong, B.W., 2021. Anthropogenic influence on 2019 May-June extremely low precipitation in Southwestern China. Bull. Am. Meteorol. Soc. 102, S97–S102. https://doi.org/10.1175/BAMS-D-20-0128.1.
Ma, Q.M., Ji, C.M., Xiong, L.H., Wang, Y., Xu, C.Y., Zhang, Y., 2021. Spatiotemporal patterns of satellite precipitation extremes in the Xijiang River Basin: from statistical characterization to stochastic behaviour modelling. Int. J. Climatol. 41, E2290–E2309. https://doi.org/10.1002/joc.6846.
Mann, H.B., 1945. Nonparametric tests against trend. Econometrica 13, 245–259. https://doi.org/10.2307/1907187.
Mirdashtvan, M., Mohseni Saravi, M., 2020. Influence of non-stationarity and auto-correlation of climatic records on spatio-temporal trend and seasonality analysis in a region with prevailing arid and semi-arid climate, Iran. J. Arid. Land 12, 964–983. https://doi.org/10.1007/s40333-020-0100-z.
O'Brien, N.L., Burn, D.H., Annable, W.K., Thompson, P.J., 2021. Trend detection in the presence of positive and negative serial correlation: A comparison of Block Maxima and Peaks-Over-threshold data. Water Resour. Res. 57, e2020WR028886 https://doi.org/10.1029/2020WR028886.
Ren, X.J., Yang, X.Q., Sun, X.G., 2013. Zonal oscillation of western Pacific subtropical high and subseasonal SST variations during Yangtze persistent heavy rainfall events. J. Clim. 26, 8929–8946. https://doi.org/10.1175/JCLI-D-12-00861.1.
Rigby, R.A., Stasinopoulos, D.M., 2005. Generalized additive models for location, scale and shape. J. R. Stat. Soc. Ser. C-Appl. Stat. 54, 507–554. https://doi.org/10.1111/j.1467-9876.2005.00510.x.
Salazar, A., Baldi, G., Hirota, M., Syktus, J., McAlpine, C., 2015. Land use and land cover change impacts on the regional climate of non-Amazonian South America: a review. Glob. Planet. Change 128, 103–119. https://doi.org/10.1016/j.gloplacha.2015.02.009.
Shankman, D., Keim, B.D., Song, J., 2006. Flood frequency in China's Poyang Lake region: trends and teleconnections. Int. J. Climatol. 26, 1255–1266. https://doi.org/10.1002/joc.1307.
Sun, F.B., Roderick, M.L., Farquhar, G.D., 2018. Rainfall statistics, stationarity, and climate change. Proc. Natl. Acad. Sci. U. S. A. 115 (10), 2305–2310. https://doi.org/10.1073/pnas.1705349115.
Tang, Y., Huang, A.N., Wu, P.L., Huang, D.Q., Xue, D.K., Wu, Y., 2021. Drivers of summer extreme precipitation events over East China. Geophys. Res. Lett. 48, e2021GL093670 https://doi.org/10.1029/2021GL093670.
Wang, H., 2020. Regional ecological risk assessment with respect to human disturbance in the Poyang Lake Region (PYLR) using Production–Living–Ecology analysis. J. Indian. Soc. Remote. Sens. 49, 449–460. https://doi.org/10.1007/s12524-020-01254-w.
Wu, D., Fang, S.B., Tong, X.Y., Wang, L., Zhuo, W., Pei, Z.F., Wu, Y.J., Zhang, J., Li, M.Q., 2021. Analysis of variation in reference evapotranspiration and its driving factors in mainland China from 1960 to 2016. Environ. Res. Lett. 16, 054016 https://doi.org/10.1088/1748-9326/abf687.
Xiao, M.Z., Zhang, Q., Singh, V.P., 2015. Influences of ENSO, NAO, IOD and PDO on seasonal precipitation regimes in the Yangtze River basin, China. Int. J. Climatol. 35, 3556–3567. https://doi.org/10.1002/joc.4228.
Xin, Z.H., Li, Y., Zhang, L., Ding, W., Ye, L., Wu, J., Zhang, C., 2019. Quantifying the relative contribution of climate and human impacts on seasonal streamflow. J. Hydrol. 574, 936–945. https://doi.org/10.1016/j.jhydrol.2019.04.095.
Xu, X.M., Tang, Q.H., 2021. Spatiotemporal variations in damages to cropland from agrometeorological disasters in mainland China during 1978–2018. Sci. Total Environ. 785, 147247 https://doi.org/10.1016/j.scitotenv.2021.147247.
Yao, J.Q., Chen, Y.N., Chen, J., Zhao, Y., Tuoliewubieke, D., Li, J.G., Yang, L.M., Mao, W.Y., 2020. Intensification of extreme precipitation in arid Central Asia. J. Hydrol. 598, 125760 https://doi.org/10.1016/j.jhydrol.2020.125760.
Yue, S., Wang, C.Y., 2002. Applicability of prewhitening to eliminate the influence of serial correlation on the Mann-Kendall test. Water Resour. Res. 38 https://doi.org/10.1029/2001WR000861, 4-1-4-7.
Zhan, M.J., Zhai, J.Q., Sun, H.M., Li, X.C., Xia, L.J., 2019. Observed exposure of population and gross domestic product to extreme precipitation events in the Poyang Lake Basin, China. Atmosphere 10 (12), 817. https://doi.org/10.3390/atmos10120817.
Zhang, X.B., Yang, F., 2004. RClimDex(1.0) User Manual. Climate Research Branch Environment Canada, Downsview, Ontario.
Zhang, Q., Xiao, M.Z., Li, J.F., Singh, V.P., Wang, Z.Z., 2014. Topography-based spatial patterns of precipitation extremes in the Poyang Lake basin, China: changing properties and causes. J. Hydrol. 512, 229–239. https://doi.org/10.1016/j.jhydrol.2014.03.010.
Zhang, Q., Xiao, M.Z., Singh, V.P., Wang, Y.Q., 2015. Spatiotemporal variations of temperature and precipitation extremes in the Poyang Lake basin, China. Theor. Appl. Climatol. 124, 855–864. https://doi.org/10.1007/s00704-015-1470-6.
Zhou, Z.Q., Xie, S.P., Zhang, R., 2021. Historic Yangtze flooding of 2020 tied to extreme Indian Ocean conditions. Proc. Natl. Acad. Sci. U. S. A. 118, e2022255118 https://doi.org/10.1073/pnas.2022255118.
Zhu, H., He, H.D., Fan, H.X., Xu, L.G., Jiang, J.H., Jiang, M.L., Xu, Y.X., 2020. Regional characteristics of long-term variability of summer precipitation in the Poyang Lake Basin and possible links with large-scale circulations. Atmosphere-Basel 11. https://doi.org/10.3390/atmos11101033.
Zou, X.K., Ren, F.M., 2015. Changes in regional heavy rainfall events in China during 1961-2012. Adv. Atmos. Sci. 32, 704–714. https://doi.org/10.1007/s00376-014-4127-y.
Zou, W.Y., Yin, S.Q., Wang, W.T., 2021. Spatial interpolation of the extreme hourly precipitation at different return levels in the Haihe River basin. J. Hydrol. 598, 126273 https://doi.org/10.1016/j.jhydrol.2021.126273.